

Continuous Rolling Motion of a Disk on a Vibrating Plate

Hiroshi Takano · Satoshi Takatori · Takatoshi Ichino

Received: date / Accepted: date

Abstract We studied the behavior of the continuous rolling motion (CRM) of a disk placed on a vibrating plate observed in the experiment using numerical simulations. Numerical simulations show that a rolling disk on a vibrating plate abruptly stops in case of pure rolling without slipping, whereas CRM occurs in the case of slipping. CRM occurs in two frequency bands separated by a gap. We use numerical simulations to determine the gap and the frequency domains for different values of the coefficient of sliding friction. The characteristics of rolling motion depend on the coefficient of slip friction and frequency of vibration.

Keywords Euler's disk · vibrating plate · continuous rolling motion · numerical simulation

PACS 45.40.-f

1 Introduction

A circular disk spinning on a rough surface is commonly observed in nature. It has been studied for centuries and still are attracting attention in recent years. If a disk is spun on a table, it keeps spinning, and then its height decreases and abruptly stop. This motion is accompanied by a rising noise

H. Takano
Educational Studies on Global-ICT-Teaching and Learning, Joetsu University of Education, Yamayashiki, Joetsu, Niigata, 943-8512, Japan
E-mail: takano@juen.ac.jp

S. Takatori
Faculty of Life and Medical Sciences, Doshisha University, Kyotanabe, Kyoto, 610-0394, Japan
E-mail: fiddich.2006-12.20@outlook.com

T. Ichino
Faculty of Biology-Oriented Science and Technology, Kindai University, Kinokawa, Wakayama, 649-6493, Japan
E-mail: ichino@waka.kindai.ac.jp

before stopping. This phenomenon is explained by the "Euler's disk", an excellent scientific toy consisting of a heavy metal disk on a slightly concave mirror[1].

Following Moffatt's discussion [2] of the abrupt halting of Euler's disk, interest increased in the finite-time singularity of a rolling disk, and a scientific discussion on the responsible dissipation mechanism began. A dissipation mechanism for a rolling friction was investigated in experimentally and theoretically. As the experimental results, trajectory of motion, the inclination angle and precession rate of the disk was measured using a high-speed video camera [3], laser beam [4], and photo-transistor [5]. The theoretical and numerical results was shown the influence of sliding, rolling, and pivoting dissipation [6–13].

On the other hand, puzzling phenomena are observed among harmonically vibrated bodies such as bouncing dimers [14] and bouncing dumbbells with chirality [15]. So disks are expected to gain energy from vibrating plate and continue to roll when they are placed on the plate. Does that really happen?

In this paper, we show the experimental and numerical results of motion of a rolling disk on a vibrating plate. As the experimental results, we observed the behavior of the continuous rolling motion (CRM) of a disk with appropriate values of frequency and amplitude of the plate. In order to reproduce the experimental results by simulation, the equations of motion of the disk on a vibrating plate were constructed. As the numerical results, continuous rolling motion of the disk does not occur under no-slip condition, however, its motion occurs under appropriate conditions with slipping.

It is very difficult to show experimentally that slipping actually occurs although the simulation shows that it is important that there is a moderate slip between the disk and plate. However, the issue is beyond the scope of this paper, and hence leave it for the future research. The aim of this

paper is simply to report the CRM in experiments and numerical simulations.

The paper is organized as follows. The experimental setup and results are shown in Sec. 2. The equations of a rolling disk on a vibrating plate are given in Sec. 3, and its numerical simulation results are shown in Sec. 4. Finally, conclusions and discussion of the results are given in Sec.5.

2 Experiment

A sketch of the setup is illustrated in Fig. 1. The plate is vibrated using an electromagnetic shaker (512 Series Vibration Generator; EMIC Co., Tokyo, Japan) shown in Fig. 1 (a). This shaker is driven by a sinusoidal waveform generator (DF1906, NF Co.) shown in Fig. 1 (b). The oscillation frequency f_r and amplitude A_m of plate oscillation are independent parameters which are changed by the power amplifier (371-A, EMIC Co.) in Fig. 1 (c). An acrylic cylinder shown in Fig. 1 (d) was attached to (a) and a disk was turned in it. The height and the diameter of the cylinder are 53 mm and 80 mm respectively. Fig. 1 (e) is an charge amplifier (505-CBP, EMIC Co.) to which an accelerometer connected.

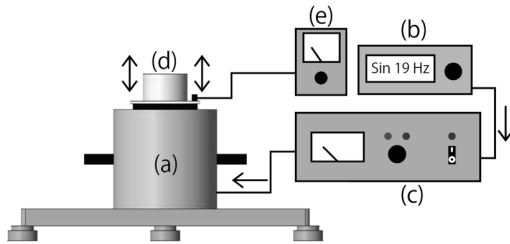


Fig. 1 Experimental setup (a) Electromagnetic shaker. (b) Waveform generator. (c) Power amplifier. (d) Acrylic cylinder. (e) Charge amplifier

The images of motion are recorded with high-speed video cameras at a frame rate of 240 fps.

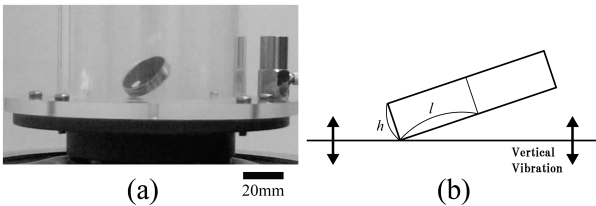


Fig. 2 (a) Photograph of the experimental setup (side view). (b) Schematic representation of the metal disk and vibrating plate where l is the radius and h is the height.

The experiments used a 25-mm-diameter, 4.95-mm-thick metal disk. Figure 2 shows a photo and a sketch of a cylindrical disk rolling on the vibrated plate.

The scientific toy ‘‘Euler’s Disk’’ rolls on its rim for up to about 90 seconds before coming abruptly to rest. On the other hand, the rolling metal disk which is used in our experiment stops within 10 s when the acrylic plate does not vibrate. However, with appropriate values of frequency and amplitude, the CRM continued for 1 min or more.

The experiment was performed with the amplitude A_m fixed and the frequency f_r changed by 1 Hz. The amplitude was changed to 0.15 mm 0.25 mm 0.375 mm and 0.5 mm. The value of the dimensionless oscillation magnitude $\Gamma = 4\pi^2 A_m f_r^2 / g$ (where g is gravitational constant) is more than unity over 32 Hz, 26 Hz and 23 Hz at the amplitude $A_m = 0.25$ mm, 0.375 mm and 0.5 mm respectively. At such high frequencies ($\Gamma > 1$), moments occur when the disc and plate are not in contact. When the disk moves away from the plate or rolls, the analysis of the motion becomes so complicated that we will not consider the phenomenon at such high frequencies here.

CRM was observed at frequencies from 13 to 15 Hz and 21 to 27 Hz at the amplitude $A_m = 0.25$ mm. The frequency was varied using 1 Hz increments with same amplitude. CRM appears to occur in these two frequency ranges, whereas no CRM occurs from 16 to 20 Hz. CRM also appears in the two frequency ranges when $A_m = 0.375$ mm and 0.5 mm. However, CRM does not occur when $A_m = 0.15$ mm. Table 1 shows the values of the frequency of two ranges when $A_m = 0.25$ mm, 0.375 mm and 0.5 mm:

Table 1 The values of the frequency of two ranges.

Amplitude (mm)	frequency (Hz)	frequency (Hz)
0.25	13~15	21~27
0.375	11~15	19~25
0.5	10~14	18~22

Figures 3 (a) and (b) show a series of snapshots of the CRM with a time interval of 5 s and 1/120 s respectively. The amplitude A_m is 0.375 mm and the frequency is 19 Hz.

3 Rolling disk model on a Vibrating Plate

3.1 Kinematics

Let’s consider the mathematical model of CRM. As shown in Fig. 4 (a), the absolute coordinate frame $(O, \mathbf{W}_{i=1,2,3})$ is fixed to the table and the coordinate frame $(O', \mathbf{E}_{i=1,2,3})$ is fixed to the vibrating plate. We consider a disk of radius l and height h . The center of mass is denoted as G and the contact point between the disk and the plate is denoted as

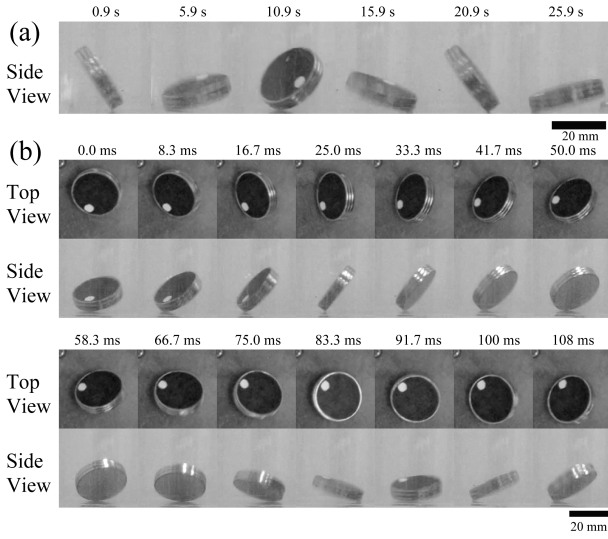


Fig. 3 (a) Snapshots of CRM separated by 5 s. The disk is rotated by hand. The time when the disk seems to be separated from the hand is set to 0 s. (b) Snapshots of CRM from 6.96 s separated by 1/120 s.

P . The tangent to the circle delimiting the disk's bottom surface at the point P is denoted as S . We introduce the frame $(O', \mathbf{E}'_{i=1,2,3})$ such that the vector \mathbf{E}'_1 is parallel to the line S . This frame is obtained by rotating the frame \mathbf{E}_i through the angle α about \mathbf{E}_3 as follows.

$$\begin{aligned} \mathbf{E}'_1 &= \cos \alpha \mathbf{E}_1 + \sin \alpha \mathbf{E}_2 \\ \mathbf{E}'_2 &= -\sin \alpha \mathbf{E}_1 + \cos \alpha \mathbf{E}_2, \quad \mathbf{E}'_3 = \mathbf{E}_3. \end{aligned}$$

Furthermore, as shown in Fig. 4 (b), we introduce the frame with the unit vectors \mathbf{e}'_i which is obtained by rotating frame \mathbf{E}'_i through the angle β about \mathbf{E}'_1 as follows.

$$\begin{aligned} \mathbf{e}'_2 &= \cos \beta \mathbf{E}'_2 + \sin \beta \mathbf{E}'_3, \\ \mathbf{e}'_3 &= -\sin \beta \mathbf{E}'_2 + \cos \beta \mathbf{E}'_3, \quad \mathbf{e}'_1 = \mathbf{E}'_1. \end{aligned}$$

The unit vectors \mathbf{e}_i are along the principal axes of the disk and are obtained by rotating the unit vectors \mathbf{e}'_i through the angle γ about $\mathbf{e}'_2 = \mathbf{e}_2$ as follows.

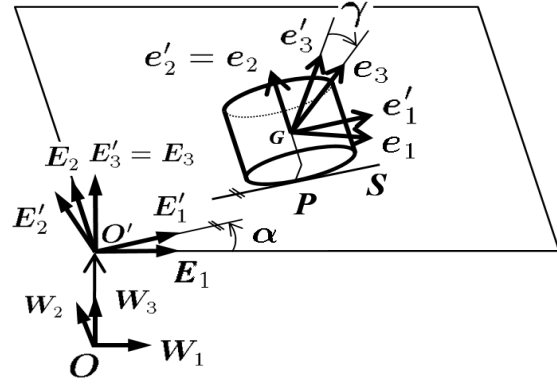
$$\begin{aligned} \mathbf{e}_1 &= \cos \gamma \mathbf{e}'_1 - \sin \gamma \mathbf{e}'_3, \\ \mathbf{e}_3 &= \sin \gamma \mathbf{e}'_1 + \cos \gamma \mathbf{e}'_3, \quad \mathbf{e}_2 = \mathbf{e}'_2. \end{aligned}$$

The disk has mass m , and the principal moments of inertia with respect to the center of mass G are $I_1 = I_3 = ml^2 k_1$ and $I_2 = ml^2 k_2$, where $k_1 \equiv \frac{1}{4} + \frac{h^2}{12l^2}$ and $k_2 \equiv \frac{1}{2}$ are dimensionless parameters. The gravitational acceleration g points in the negative \mathbf{E}_3 direction.

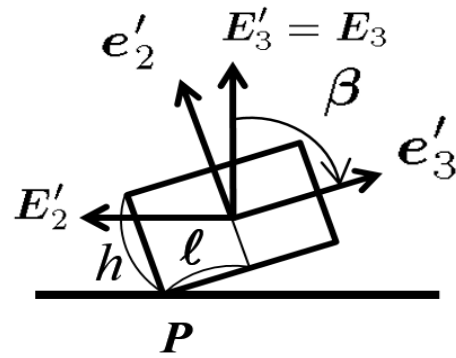
The position vectors \mathbf{r}_t , \mathbf{r} , \mathbf{r}_0 , \mathbf{r}_g and \mathbf{R}_g are shown in Fig. 5. The vector \mathbf{r}_t has the following components:

$$\begin{aligned} \mathbf{r}_t &= x\mathbf{E}'_1 + y\mathbf{E}'_2 = (x, y, 0)_{\mathbf{E}'} \\ &= (x \cos \alpha - y \sin \alpha, x \sin \alpha + y \cos \alpha, 0)_{\mathbf{E}}. \end{aligned}$$

In the following, we use subscripts such as \mathbf{E}' and \mathbf{E} to identify the frame in which the components are represented.



(a)



(b)

Fig. 4 (a) Definition of the coordinate frames. \mathbf{W}_i is the absolute coordinate frame. \mathbf{E}_i is the coordinate frame fixed to the vibrating plate and \mathbf{E}'_i is obtained by rotating the frame \mathbf{E}_i through the angle α about \mathbf{E}_3 . \mathbf{e}_i is principal axis of inertia of the disk and \mathbf{e}'_i is obtained by rotating frame \mathbf{e}_i through the angle γ about \mathbf{e}_2 . (b) \mathbf{e}'_i is also obtained by rotating frame \mathbf{E}'_i through the angle β about \mathbf{E}'_1 .

The vectors \mathbf{r} , \mathbf{r}_0 , and $\mathbf{R}_g = \mathbf{r}_0 + \mathbf{r}_t - \mathbf{r}$ have the following components:

$$\begin{aligned} \mathbf{r} &= -l\varepsilon \mathbf{e}'_2 - l\mathbf{e}'_3 = -l(0, \varepsilon, 1)_{\mathbf{e}'} = -l(0, \rho_2, \rho_3)_{\mathbf{E}'}, \\ \mathbf{r}_0 &= (0, 0, lr_0)_{\mathbf{E}}, \quad \mathbf{R}_g = (x, y + l\rho_2, l(\rho_3 + r_0))_{\mathbf{E}'}, \end{aligned}$$

where

$$\varepsilon \equiv \frac{h}{2l}, \quad \rho_2 \equiv \varepsilon \cos \beta - \sin \beta, \quad \rho_3 \equiv \varepsilon \sin \beta + \cos \beta.$$

The plate is oriented horizontally and vibrated vertically with $r_0 = A_m \sin(2\pi f_r t)/l$, where A_m is the amplitude and f_r is the oscillation frequency of the plate oscillation.

The components of angular velocity with respect to frame \mathbf{e}' are as follows:

$$\begin{aligned} \boldsymbol{\omega} &= \dot{\gamma} \mathbf{e}'_2 + \dot{\beta} \mathbf{e}'_1 + \dot{\alpha} \mathbf{E}_3 = (\omega_1, \omega_2, \omega_3)_{\mathbf{e}'}, \\ &= (\dot{\beta}, \dot{\gamma} + \dot{\alpha} \sin \beta, \dot{\alpha} \cos \beta)_{\mathbf{e}'}. \end{aligned} \quad (1)$$

The overhead dot symbol denotes differentiation with respect to time.

The inertia tensor is diagonal when expressed in the body fixed frame, or in a corotating frame \mathbf{e}' . The angular momentum

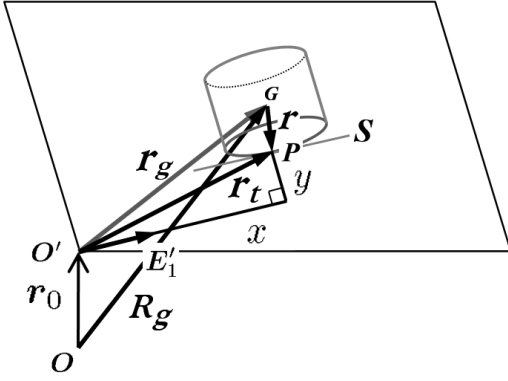


Fig. 5 The position vectors \mathbf{r}_t , \mathbf{r} , \mathbf{r}_g , \mathbf{r}_0 and \mathbf{R}_g . \mathbf{r}_t is the position vector from O' to the point of contact P , \mathbf{r} is the position vector from G to the point of contact P , \mathbf{r}_g is the position vector from O' to G , \mathbf{r}_0 is the position vector from O to O' and \mathbf{R}_g is the position vector from O to G .

\mathbf{L} is expressed in frame \mathbf{e}' such that $\mathbf{L} = ml^2(k_1\omega_1, k_2\omega_2, k_3\omega_3)_{\mathbf{e}'}$ because $k_1 = k_3$.

The time derivative of vector $\mathbf{A} = a_i\mathbf{e}_i = a'_i\mathbf{e}'_i = A'_i\mathbf{E}'_i$ is $\frac{d}{dt}\mathbf{A} = \dot{a}_i\mathbf{e}_i + \boldsymbol{\omega} \times \mathbf{A}$, hence, the components are

$$\frac{d}{dt}\mathbf{A} = (\dot{a}'_1 + (\tan\beta\dot{a}'_3 - \dot{a}'_2)\omega_3, \dot{a}'_2 + \omega_3\dot{a}'_1 - \omega_1\dot{a}'_3,$$

$$\dot{a}'_3 - \tan\beta\omega_3\dot{a}'_1 + \omega_1\dot{a}'_2)_{\mathbf{e}'}, \quad (2)$$

$$= (\dot{A}'_1 - \dot{\alpha}A'_2, \dot{A}'_2 + \dot{\alpha}A'_1, \dot{A}'_3)_{\mathbf{E}'}. \quad (3)$$

The slip velocity of the contact point P is defined as $\mathbf{v}_p \equiv \frac{d}{dt}\mathbf{r}_t - \dot{r}_i\mathbf{e}_i$ and is denoted as follows:

$$\mathbf{v}_p = l(V_{p1}, V_{p2}, 0)_{\mathbf{E}'} = (\dot{x} - \dot{\alpha}y - l\dot{\gamma}, \dot{y} + \dot{\alpha}x, 0)_{\mathbf{E}'}. \quad (4)$$

The first term $\frac{d}{dt}\mathbf{r}_t$ denotes the velocity of the contact point P as seen by the observer on the plate fixed to frame \mathbf{E} , and the second term $\dot{r}_i\mathbf{e}_i$ denotes the contact point P as seen by the observer on the disk fixed to frame \mathbf{e} .

The time derivative of \mathbf{R}_g gives the velocity of the center of mass, $\mathbf{v}_g \equiv \frac{d}{dt}\mathbf{R}_g = l(V_{g1}, V_{g2}, V_{g3})_{\mathbf{E}'}$, as follows:

$$\mathbf{v}_g = \frac{d}{dt}\mathbf{r}_t - (\dot{r}_i\mathbf{e}_i + \boldsymbol{\omega} \times \mathbf{r}) + \frac{d}{dt}\mathbf{r}_0$$

$$= \mathbf{v}_p - \boldsymbol{\omega} \times \mathbf{r} + \frac{d}{dt}\mathbf{r}_0 \quad (4)$$

$$= l(V_{p1} + \omega_2 - \varepsilon\omega_3, V_{p2} - \omega_1\rho_3, \omega_1\rho_2 + \dot{r}_0)_{\mathbf{E}'}. \quad (5)$$

The time derivative of the angular momentum \mathbf{L} is obtained from Eq. (2):

$$\frac{d}{dt}\mathbf{L} = ml^2(k_1\dot{\omega}_1 + k_1\tan\beta\omega_3^2 - k_2\omega_2\omega_3, k_2\dot{\omega}_2,$$

$$k_1\dot{\omega}_3 - k_1\tan\beta\omega_1\omega_3 + k_2\omega_1\omega_2)_{\mathbf{e}'}. \quad (6)$$

3.2 Equations of motion

The equations of motion can be expressed as

$$\frac{d}{dt}\mathbf{L} = \mathbf{r} \times \mathbf{f}, \quad (7)$$

$$m\frac{d}{dt}\mathbf{v}_g = \mathbf{f} - mg\mathbf{E}_3, \quad (8)$$

where \mathbf{f} and \mathbf{M}_f are the reaction force to the plate and the moment of rolling friction, respectively. Because any body is deformable, the actual contact between the body and the horizontal plane will involve a contact region rather than a single point. The moment \mathbf{M}_f is intended to incorporate the effects of a finite region of contact.

According to Leine [12], who studied the abrupt halting of the rolling disk, the moment of rolling friction \mathbf{M}_f contains classical rolling friction, contour friction, pivoting friction, and friction due to viscous air drag. Contour friction is a resisting moment against the movement of the contact point over the rim of the disk [10, 12]. Leine concluded that contour friction is the predominant contributor to the friction causing the abrupt halt.

The energy dissipation due to the contour friction E_{diss} is considered to be proportional to the product of the normal force mlf_N which is assumed to be almost constant and the distance $D = l|\dot{\gamma}|$ at which the contact point moves

$$E_{diss} = -\mu_c m l f_N D, \quad (9)$$

so that the rate of dissipation of energy is

$$\frac{d}{dt}E_{diss} = -\mu_c m l^2 f_N \dot{\gamma} \text{sgn}(\dot{\gamma}), \quad (10)$$

where μ_c is the friction coefficient of contour friction. On the other hand, the rate of dissipation of energy is calculated by

$$\frac{d}{dt}E_{diss} = \boldsymbol{\omega} \cdot \mathbf{M}_f. \quad (11)$$

Comparing Eq. (10) and Eq. (11) leads to

$$\mathbf{M}_f = \mu_c m l^2 f_N \text{sgn}(\dot{\gamma})(0, -1, \tan\beta)_{\mathbf{e}'}. \quad (12)$$

As for rolling without slipping, the vanishing slip velocity $\mathbf{v}_p = 0$ leads to $\mathbf{v}_g = \mathbf{r} \times \boldsymbol{\omega} + \frac{d}{dt}\mathbf{r}$ from Eq. (4). By using Eq. (8), the reaction force is obtained

$$\mathbf{f} = m \left(\frac{d}{dt}(\mathbf{r} \times \boldsymbol{\omega}) + (g + l\ddot{r}_0)\mathbf{E}_3 \right). \quad (12)$$

Substituting Eq. (12) into Eq. (7) and using Eq. (2) gives

$$k'_1\dot{\omega}_1 + g'\rho_2 = (k'_2 + \varepsilon\tan\beta)\omega_2\omega_3 - (k'_1\tan\beta + \varepsilon)\omega_3^2,$$

$$k'_2\dot{\omega}_2 - \varepsilon\dot{\omega}_3 = -(1 + \varepsilon\tan\beta)\omega_1\omega_3 - f_N\mu_c\text{sgn}(\dot{\gamma}),$$

$$k'_1\dot{\omega}_3 - \varepsilon\dot{\omega}_2 = (k'_1\tan\beta + \varepsilon)\omega_1\omega_3 - k_2\omega_1\omega_2 + f_N\mu_c\tan\beta\text{sgn}(\dot{\gamma}),$$

where

$$k'_1 \equiv k'_1 + 1, \quad k'_1 \equiv k_1 + \varepsilon^2, \quad k'_2 \equiv k_2 + 1, \quad g' \equiv \dot{r}_0 + \frac{g}{l}.$$

Using Eq. (8) and Eq. (5), we obtain the normal force of

$$f_N \equiv \frac{\mathbf{f}_N \cdot \mathbf{E}_3}{ml} = \dot{\omega}_1\rho_2 - \omega_1^2\rho_3 + g'.$$

As for rolling with slipping, the force \mathbf{f} is given by the sum of the normal contact force \mathbf{f}_N and the sliding friction force \mathbf{f}_s . We adopt the Coulomb friction force given by

$$\mathbf{f}_s = -ml\mu_s f_N (\hat{V}_{p1}, \hat{V}_{p2}, 0)_{\mathbf{E}'}, \quad (13)$$

where

$$\hat{V}_{p1} \equiv \frac{V_{p1}}{\sqrt{\mathbf{V}_p^2 + \varepsilon_c^2}}, \hat{V}_{p2} \equiv \frac{V_{p2}}{\sqrt{\mathbf{V}_p^2 + \varepsilon_c^2}},$$

μ_s is the coefficient of sliding friction, and ε_c is a sufficiently small parameter to make this force vanish at $\mathbf{V}_p = 0$. According to the Coulomb-Contensou friction model, this small parameter can be attributed to a non-zero pivot angular velocity ω_3 while the disk is spinning.[16–19]

Substitution of Eq. (13) and Eq. (6) into Eq. (7) gives the following equations:

$$\begin{aligned} k_1 \dot{\omega}_1 &= -k_1 \tan \beta \omega_3^2 + k_2 \omega_2 \omega_3 - f_N (\mu_s \rho_3 \hat{V}_{p2} + \rho_2), \\ k_2 \dot{\omega}_2 &= f_N (\mu_s \hat{V}_{p1} - \mu_c \operatorname{sgn}(\dot{\gamma})), \\ k_1 \dot{\omega}_3 &= k_1 \tan \beta \omega_1 \omega_3 - k_2 \omega_1 \omega_2 \\ &\quad - f_N (\varepsilon \mu_s \hat{V}_{p1} - \mu_c \tan \beta \operatorname{sgn}(\dot{\gamma})). \end{aligned}$$

Using Eq. (3) and substituting Eq. (5) and Eq. (13) into Eq. (8) gives

$$\begin{aligned} \dot{V}_{p1} + \dot{\omega}_2 - \varepsilon \omega_3 &= \frac{\omega_3}{\cos \beta} (V_{p2} - \omega_1 \rho_3) - f_N \mu_s \hat{V}_{p1}, \\ \dot{V}_{p2} - \dot{\omega}_1 \rho_3 &= \omega_1^2 \rho_2 - \frac{\omega_3}{\cos \beta} (V_{p1} + \omega_2 - \varepsilon \omega_3) - f_N \mu_s \hat{V}_{p2}. \end{aligned}$$

4 Simulation

We simulated the disk's motion on the vibrating plate using the equations of motion obtained above. For the numerical simulations, the NDSolve command in *Mathematica* (Wolfram Research Inc.) is used.

If the disk is pure rolling without slipping ($\mathbf{V}_p = 0$) and the plate is not vibrating, there is a motion that rotates without moving the center of mass. This type of motion is called stationary rolling motion, being characterized by

$$\mathbf{V}_g = 0, \quad \omega_2 = \varepsilon \omega_3, \quad \omega_3^2 = \frac{g(\sin \beta_0 - \varepsilon \cos \beta_0)}{l(k_1 \tan \beta_0 - \varepsilon k_2)}, \quad (14)$$

where the angle β_0 is given by an initial constant value. If this motion is perturbed, the angle β oscillates around an equilibrium position β_0 . This oscillation is called nutation. According to Leine [12], the nutation frequency f_n around stationary rolling motion with angle β is given by

$$f_n = \frac{1}{2\pi} \sqrt{\frac{g(3k_1 \tan^2 \beta + 1) \cos \beta}{lk_1(k_1 + 1)}}.$$

We find that CRM occurs when the vibration frequency of the plate approaches the nutation frequency.

We used the following parameter values and initial conditions for the simulations:

$$\begin{aligned} g &= 9810 \text{ mm/sec}^2, \quad A_m = 0.25 \text{ mm}, 0.375 \text{ mm}, 0.5 \text{ mm}, \\ l &= 12.5 \text{ mm}, \quad h = 4.95 \text{ mm}, \\ \alpha(0) &= 0^\circ, \beta(0) = 60^\circ, \gamma(0) = 0^\circ, \\ \boldsymbol{\omega}(0) &= (0, -8.1, -41.1)_e \text{ rad/s}, \end{aligned}$$

where the values of angular velocity correspond to the stationary rolling motion for the angle $\beta(0) = 60^\circ$ which are obtained from Eq. (14). The contour friction coefficient was set to $\mu_c = 0.0013$, which is obtained by comparing the time taken to halt as determined via the numerical simulation with that observed experimentally under the no vibration conditions. As the goal of the present work is to discuss continuous rolling in qualitative terms, an accurate value of the coefficient of contour friction is not necessary.

4.1 no-slip case

We studied the disk's motion without slipping at the amplitude $A_m = 0.25$ mm.

Figure 6 shows the angle β as a function of time for various vibrating frequencies. An abrupt halt was observed, similar to that which occurs with no vibration, up to the frequency $f_r = 36$ Hz. The halt occurred, although large beats occurred at the frequency $f_r = 11$ Hz, which is near the nutation frequency for the angle $\beta = 60^\circ$. The same large beats and halt appeared at the frequency $f_r = 24$ Hz near twice the nutation frequency.

Above the frequency $f_r = 32$ Hz ($\Gamma > 1$) for the amplitude $A_m = 0.25$ mm, the normal reaction force became negative in the last period of rolling which means that moments occur when the disc and plate are not in contact, as can be checked through simulation. Thus the simulations at the frequencies more than 32 Hz ($\Gamma > 1$) is not considered in the following.

We studied cases for various values of the coefficient of contour friction: $\mu_c = 0.1, 0.01, 0.0001$ and the amplitude $A_m = 0.375$ mm, 0.5 mm. The results thus obtained were similar to those for $\mu_c = 0.0013$, and CRM was not observed.

4.2 slipping case

We simulated the disk in stationary rolling motion with slipping on a vibrating plate.

For a small coefficient of sliding friction that was less than μ_s^{\min} and for a large one that was more than μ_s^{\max} , CRM did not occur in the frequency range from 8 to 35 Hz. But CRM occurred for the value of coefficient of sliding friction from μ_s^{\min} to μ_s^{\max} . CRM does not occur when it is either slippery or not slippery at all; in other words, for CRM, a domain of appropriate values exist in the space defined by the vibrating frequency and the coefficient of sliding friction. Table 2 shows the value of μ_s^{\min} and μ_s^{\max} at the amplitude $A_m = 0.25$ mm, 0.375 mm and 0.5 mm.

The domains where CRM occurs are shown in Fig. 7 (a), (b) and (c) at the amplitude $A_m = 0.25$ mm, 0.375 mm and 0.5 mm respectively. The plotted points indicate where the

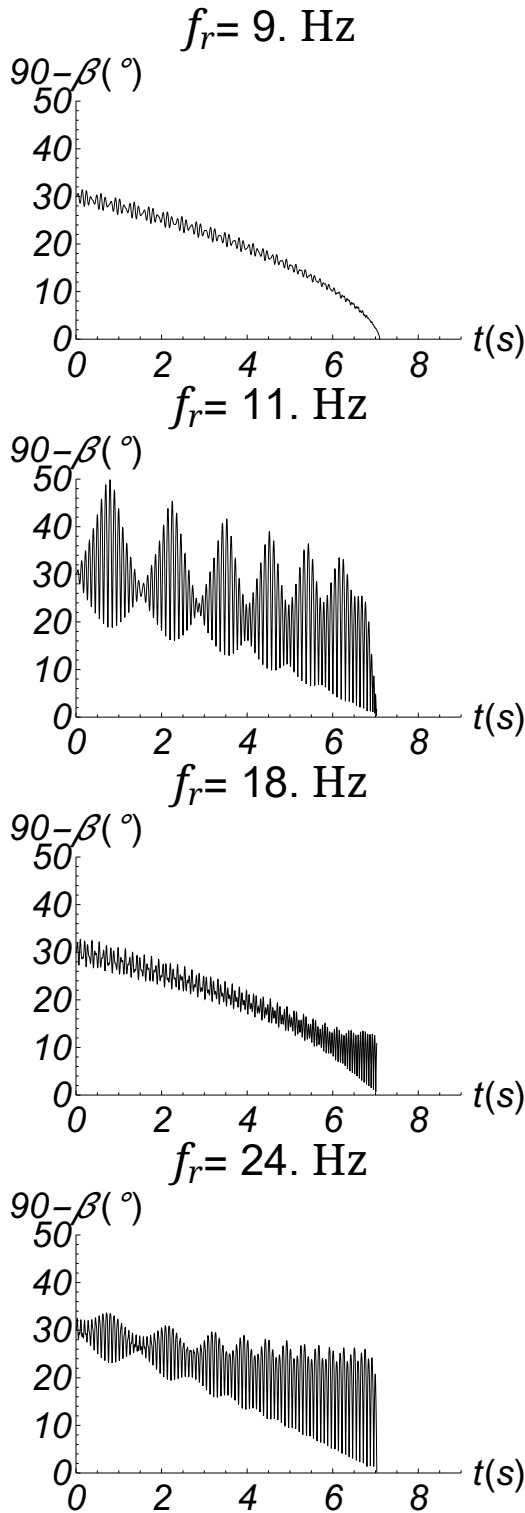


Fig. 6 Angle β in the simulation for rolling without slipping.

Table 2 The value of μ_s^{min} and μ_s^{max} .

A_m (mm)	0.25	0.375	0.5
μ_s^{min}	0.0195	0.00859	0.00892
μ_s^{max}	0.202	0.233	0.233

disk continues rotating for 120 s. The lines show the values obtained in the experiment (Table 1). The simulation reveals two subdomains separated by a frequency gap. The low-frequency domain extends to nearly the nutation frequency and the high-frequency domain extends to nearly twice the value of the nutation frequency. Fig. 7 (a), (b) and (c) indicate that the range of frequencies obtained in the experiment almost coincides with the domain shown in the simulation even though the simulation only includes the contour friction and sliding friction.

Figure 8 shows the typical behavior of the angle β as a function of time where the amplitude A_m is 0.375 mm and the vibrating frequency f_r is 25 Hz. In the first period up to about 2.5 seconds, the angle β behaves like the angle in stationary rolling motion in the no-slip case, and decreases gradually. The motion of the disk shifts to CRM after about 3 seconds, and the amplitude of the nutation oscillation is almost constant; the nutation fluctuation range of the angle β is about $10^\circ \sim 29^\circ$.

Figure 9 shows the behavior of the angle β over a short time interval $t = 6.02 \sim 6.24$ seconds in Fig. 8. The images in the Fig. 9 are extracted every four frames (0.0167 seconds) from an experiment movie under the same conditions as the simulation. Grid lines are drawn at the same time intervals. It is found that the period of the nutation oscillation in the simulation reproduces the period in the experiment.

Figure 10, 11 and 12 show the angle β as a function of time for various vibrating frequencies at the amplitude $A_m = 0.25$ mm, 0.375 mm and 0.5 mm respectively. We used a coefficient of sliding friction $\mu_s = 0.11$, 0.09, and 0.07 at the amplitude $A_m = 0.25$ mm, 0.375 mm and 0.5 mm respectively. These values were determined based on a large overlap between the ranges in the experiment and the domains in the simulation in Fig. 7. The behaviors of the angle β are not CRM at the frequency 31 Hz in the amplitude $A_m = 0.375$ mm and at the frequency 28 Hz in the amplitude $A_m = 0.5$ mm, because the normal force becomes negative from the time $t \sim 5$ seconds, as can be checked through simulation.

Table 3 shows the nutation fluctuation range of the angle β at the amplitudes of the plate ($A_m = 0.25, 0.375, 0.5$ mm) and at frequency 11, 14 Hz (low-frequency domain) and 22 Hz, 25 Hz (high-frequency domain). The width of the range is approximately equal even if the amplitude changes at each frequency. In both the low-frequency domain and the high-frequency domain, the widths of the range become narrower

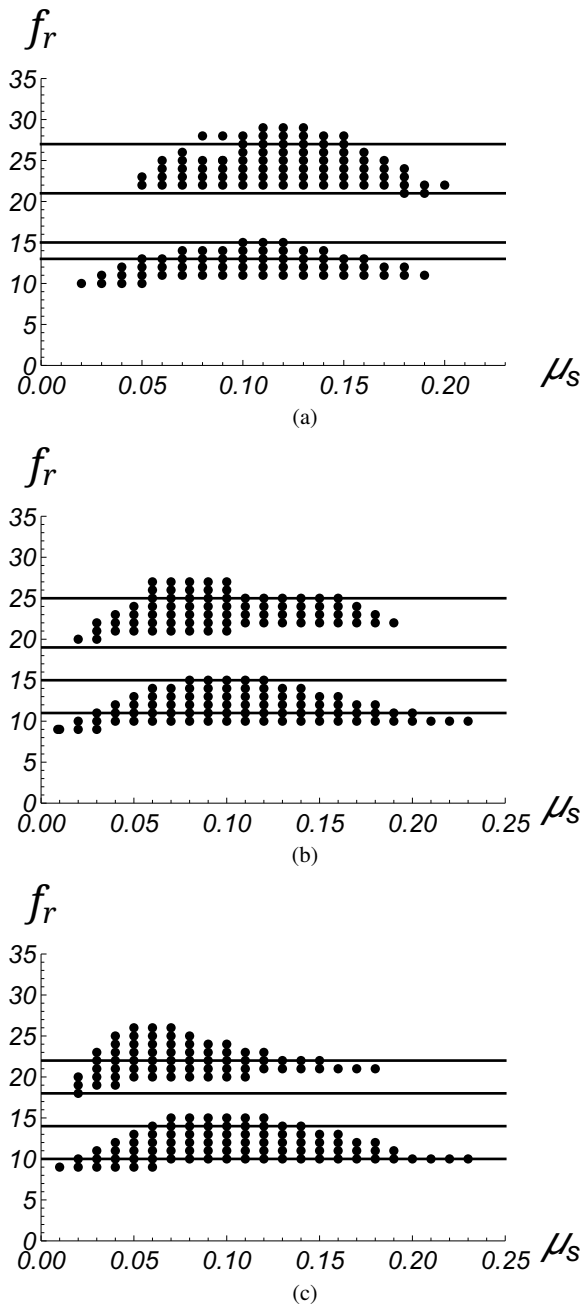


Fig. 7 The domain of CRM as a function of frequency f_r and coefficient of slip friction μ_s . (a) Amplitude $A_m = 0.25$ mm. (b) Amplitude $A_m = 0.375$ mm. (c) Amplitude $A_m = 0.5$ mm.

and the minimum values of the angle become small as the frequency increases.

Table 3 The nutation fluctuation range of the angle β .

A_m (mm)	11 Hz	14 Hz	22 Hz	25 Hz
0.25	$17^\circ \sim 37^\circ$	$6^\circ \sim 24^\circ$	$15^\circ \sim 37^\circ$	$9^\circ \sim 29^\circ$
0.375	$16^\circ \sim 39^\circ$	$4^\circ \sim 26^\circ$	$16^\circ \sim 37^\circ$	$6^\circ \sim 30^\circ$
0.5	$16^\circ \sim 41^\circ$	$4^\circ \sim 27^\circ$	$18^\circ \sim 36^\circ$	$10^\circ \sim 29^\circ$

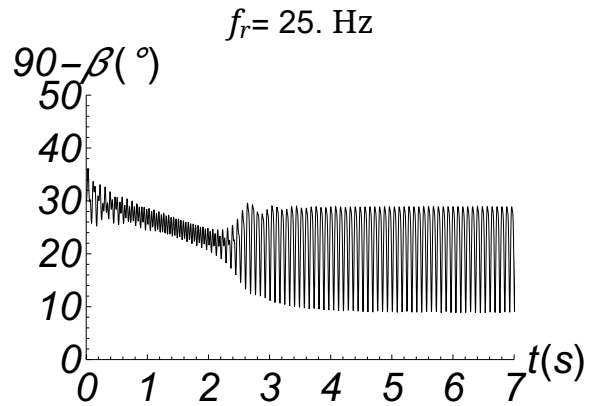


Fig. 8 The typical behavior of the angle β at the amplitude $A_m = 0.375$ mm and at the vibrating frequency $f_r = 25$ Hz.

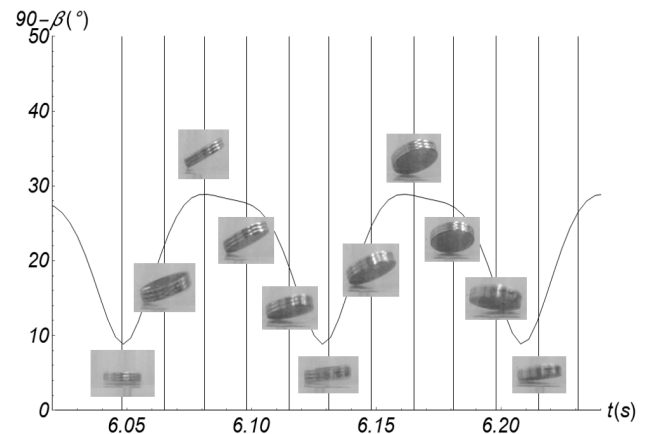


Fig. 9 The angular behavior of angle β over a short time interval $t = 6.02 \sim 6.24$ seconds in Fig. 8.

5 Conclusion and discussion

To summarize our experiments, when vertical vibrations are applied to a rolling disk, CRM occurs with appropriate values of frequency and amplitude. In the numerical simulation, the CRM of the disk does not occur on the vibrating plate under no-slip conditions; however, CRM does occur under appropriate conditions with slipping. In the experiment, CRM occurs in two frequency ranges separated by a gap, and we use numerical simulations to confirm the gap and the frequency domains for different values of the coefficient of sliding friction.

It is found out that slipping is important on the result of the simulation. However, we have not ascertained whether the disk actually slip. Thus, it is a future subject to investigate slipping using some direct method. Slipping seems to synchronize the oscillation of the angle β and that of the plate, which leads to the CRM of the disk. It is also a future subject to clear how this synchronization happens and why the two frequency bands appear.

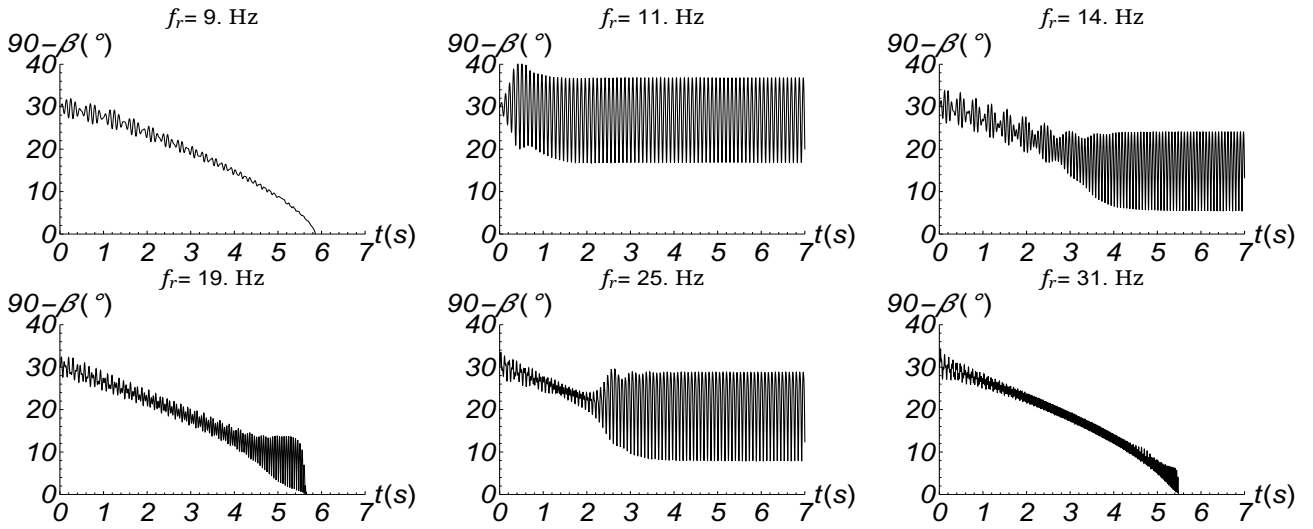


Fig. 10 Angle β in the simulation with slipping at the amplitude $A_m = 0.25$ mm. The coefficient of slip friction $\mu_s = 0.11$.

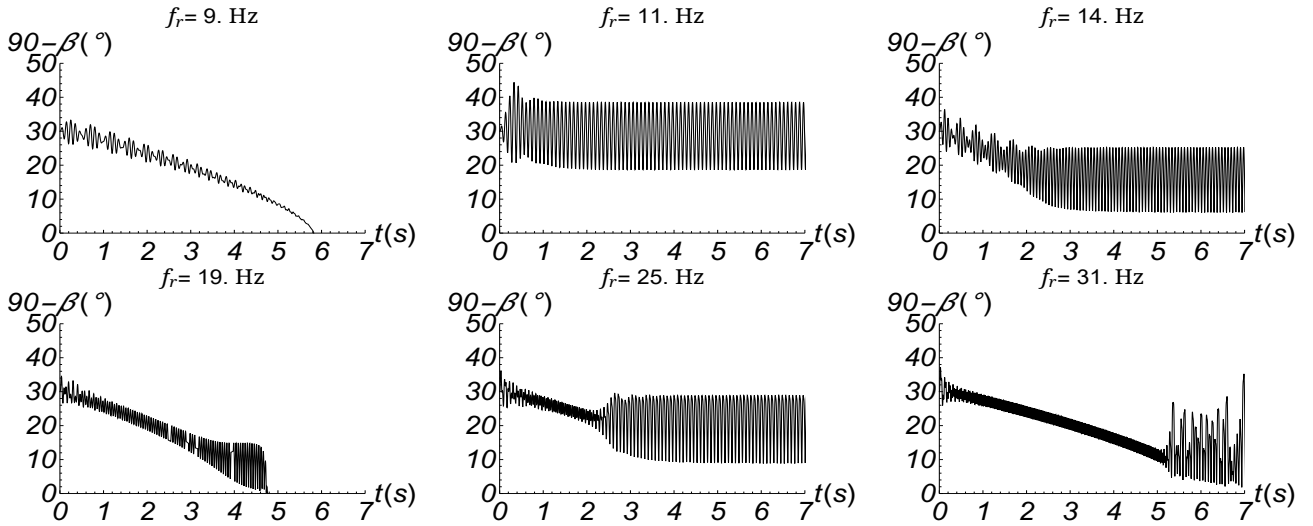


Fig. 11 Angle β in the simulation with slipping at the amplitude $A_m = 0.375$ mm. The coefficient of slip friction $\mu_s = 0.09$.

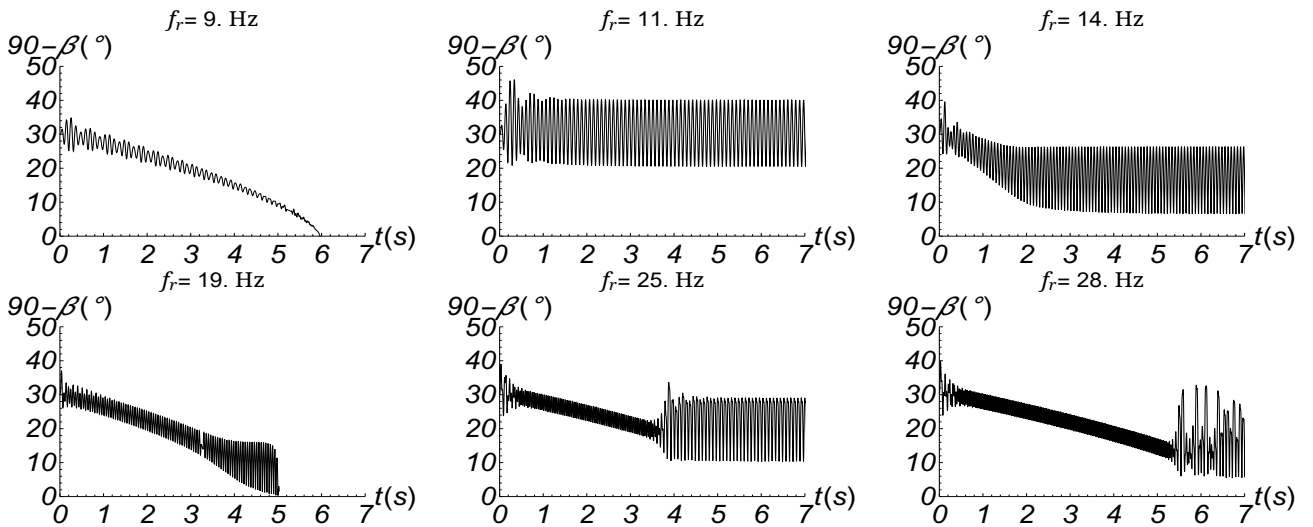


Fig. 12 Angle β in the simulation with slipping at the amplitude $A_m = 0.5$ mm. The coefficient of slip friction $\mu_s = 0.07$.

Conflict of interest

The authors declare that they have no conflict of interest.

References

1. Bendik, J., The official Euler's disk website. <http://www.eulersdisk.com> (2000). Accessed 28 Feb. 2020
2. Moffatt, H. K., Euler's disk and its finite-time singularity, *Nature(London)*, vol. 404, pp. 833.(2000)
3. Easwar, K., Rouyer, F., Menon, N., Speeding to a stop: the finite-time singularity of a spinning disk., *Phys. Rev. E*, vol. 66(3), 045102(R).(2002)
4. Caps, H., Dorbolo, S., Ponte, S., Croisier, H. and Vandewalle, N., Rolling and slipping motion of Euler's disk, *Phys. Rev. E*, 2004, vol. 69, 056610.(2004)
5. McDonald, A. J., McDonald, K. T., The rolling motion of a disk on a horizontal plane, Preprint Archive. Los Alamos National Laboratory. arXiv:Physics/008227 (2000)
6. Kessler, P. and O' Reilly, O. M., The Ringing of Euler's Disk, *Regul. Chaotic Dyn.*, vol. 7, pp. 49–60.(2002)
7. O' Reilly, O. M., The Dynamics of Rolling Disks and Sliding Disks, *Nonlinear Dyn.*, vol. 10(3), pp. 287–305.(1996)
8. Stanislavsky, A. A., Weron, K., Nonlinear oscillations in the rolling motion of Euler's disk, *Physica D*, vol. 156, pp. 247–259.(2001)
9. Borisov, A. V., Mamaev, I. S. and Kilin, A. A., Dynamics of Rolling Disk, *Regul. Chaotic Dyn.*, vol. 8, pp. 201–212.(2003)
10. Le Saux, C., Leine, R. I. and Glocker, C., Dynamics of a Rolling Disk in the Presence of Dry Friction, *J. Nonlinear Sci.*, vol. 15, pp. 27–61.(2005)
11. Leine, R. I. Le Saux, C. and Glocker, C., Friction models for the rolling disk, In Proceedings of the ENOC 2005 Conference (August 7-12 2005). Eindhoven, CD-ROM
12. Leine, R. I., Experimental and theoretical investigation of the energy dissipation of a rolling disk during its final stage of motion, *Arch. Appl. Mech.*, vol. 79, pp. 1063–1082.(2009)
13. Ma, D., Liu, C., Zhao, Z. and Zhang, H., Rolling friction and energy dissipation in a spinning disc., *Proc. R. Soc. A*, vol. 470, pp. 20140191.(2014)
14. Dorbolo, S., Volfson, D. Tsimring, L. and Kudrolli, L., Dynamics of a Bouncing Dimer, *Phys. Rev. Lett.*, vol. 95, pp. 044101.(2005)
15. Kubo, Y., Inagaki, S., Ichikawa, M. and Yoshikawa, K., Mode bifurcation of a bouncing dumbbell with chirality, *Phys. Rev. E*, vol. 91, pp. 052905.(2015)
16. Zhuravlev, V. G., The model of dry friction in the problem of the rolling of rigid bodies, *J. Appl. Maths. Mechs*, vol. 62, pp. 705–710.(1998)
17. Leine, R. I., Glocker, C., A set-valued force law for spatial Coulomb-Contensou friction, *Eur. J. Mech. A Solids*, vol. 22, pp. 193–215.(2003)
18. Kireenkov, A. A., Combined Model of Sliding and Rolling Friction in Dynamics of Bodies on a Rough Plane, *Mech. Solids (Engl. Transl.)*, vol. 43, pp. 412–425.(2008)
19. Kudra, G., Awrejcewicz, J., Approximate modelling of resulting dry friction forces and rolling resistance for elliptic contact shape, *Eur. J. Mech. A Solids*, vol. 42, pp. 358–375.(2013)